WILEY InterScience® DISCOVER SOMETHING GREAT

Multilevel Numerical Solutions of Convection-Dominated Diffusion Problems by Spline Wavelets

Jiangguo Liu,[1] **Richard E. Ewing,**[2] **Guan Qin**[2]
[1] *Department of Mathematics, Colorado State University, Fort Collins, Colorado 80523-1874*

[2] *Institute for Scientific Computation, Texas A&M University, College Station, Texas 77843-3404*

Received 31 July 2005; accepted 25 September 2005
Published online 30 November 2005 in Wiley InterScience (www.interscience.wiley.com).
DOI 10.1002/num.20132

In this article, we utilize spline wavelets to establish an adaptive multilevel numerical scheme for time-dependent convection-dominated diffusion problems within the frameworks of Galerkin formulation and Eulerian-Lagrangian localized adjoint methods (ELLAM). In particular, we shall use linear Chui-Quak semi-orthogonal wavelets, which have explicit expressions and compact supports. Therefore, both the diffusion term and boundary conditions in the convection-diffusion problems can be readily handled. Strategies for efficiently implementing the scheme are discussed and numerical results are interpreted from the viewpoint of nonlinear approximation. © 2005 Wiley Periodicals, Inc. Numer Methods Partial Differential Eq 22: 994–1006, 2006

Keywords: boundary value problem; characteristic tracking; convection-diffusion equation; nonlinear approximation; semi-orthogonal; spline; wavelet

I. INTRODUCTION

Many applications in sciences and engineering demand multiscale modeling and computations. As we know, wavelets are tightly connected with multiresolution analyses, which provide a platform for performing multilevel computations. Efforts in applying wavelets to solve differential and integral equations can be observed in [1–3], as well as in many other articles. Previously, we applied compactly supported orthogonal and biorthogonal wavelets to establish unconditionally stable explicit numerical schemes for convection-reaction equations [4, 5] within the frameworks of Galerkin methods and ELLAM [6].

For approximations based on wavelets, the order of accuracy is usually the number of vanishing moments of the wavelets being used. Given the number of vanishing moments, the Daubechies' orthogonal wavelets [7] have minimal supports and, hence, require less computations (theoretically). But these wavelets lack closed forms. The primals of the biorthogonal wavelets developed

Correspondence to: Jiangguo Liu, Department of Mathematics, Colorado State University, Fort Collins, CO 80523-1874 (email: liu@math.colostate.edu)

© 2005 Wiley Periodicals, Inc.

in [8] are splines and hence have explicit expressions, but the duals do not. For some applications, wavelet coefficients are computed through numerical integrations on the wavelet supports. So minimal support is a good thing to have, but one has to store many point values of the wavelets in their supports (usually at dyadic points) if the wavelets lack explicit expressions. For Lagrangian or semi-Lagrangian methods [6,9], the feet of characteristics are not necessarily dyadic points, so interpolation between dyadic points must be taken into consideration. In addition, these orthogonal or biorthogonal wavelets are bases for the whole real line, instead of bounded intervals. Periodization of these wavelets might be suitable for image processing, but not necessarily so for boundary value problems of differential equations. Another nuisance in dealing with these wavelets is from their derivatives. Obviously, the derivatives do not possess explicit expressions either, so it is hard to apply these wavelets directly to diffusion problems, which involve second-order derivatives of unknown functions, or first-order derivatives of test and trial functions if the Galerkin formulation is applied. Some investigators proposed using eigenvectors and refinement equations to handle integrals of wavelet derivatives [10], but it is preferable to have a direct treatment.

Bearing with these concerns, we turn to the semi-orthogonal spline wavelets developed by Chui and Quak in [11]. These spline wavelets form bases on bounded intervals, and have compact supports and explicit expressions, so the above issues for solving differential equations by wavelets are readily resolved. The duals of these wavelets are fully supported on the whole intervals, but are not really needed in our applications. In this article, we shall use these spline wavelets as both trial and test functions within the Galerkin framework to solve convection-diffusion equations.

We want to point out that these semi-orthogonal spline wavelets have been used to solve first-kind integral equations in [3]. A nice comparison between orthogonal and semi-orthogonal wavelets for solving integral equations is presented in [12]. The advantages of semi-orthogonal spline wavelets have also been exploited in [13] to solve inverse problems for two-phase flows in porous media. Castano and Kunoth have recently used these spline wavelets on robust regression of scattered data [14]. Discussions on how to apply these wavelets to nonlinear problems can be found in [15].

The rest of this article is organized as follows. Section 2 presents the differential equations to be solved and the main ideas of the ELLAM methodology. The features of Chui-Quak semi-orthogonal spline wavelets are briefly reviewed in Section 3. Section 4 establishes our multilevel numerical scheme for convection-dominated diffusion equations by applying these spline wavelets within the frameworks of Galerkin formulation and ELLAM. Strategies for efficient implementations and numerical results are presented in Section 5. Section 6 concludes the article with some brief remarks.

II. ELLAM FOR CONVECTION-DIFFUSION PROBLEMS

ELLAM is a general framework for convection-diffusion-reaction equations. Finite element methods, collocation methods, and wavelet methods have been developed within this framework [5, 16, 17]. An excellent overview about the current state of research on ELLAM is given in [18]. In this article, we focus on convection-diffusion equations in one-dimensional space, but the notations used are consistent with those for multiple dimensions.

$$\begin{cases} u_t + \nabla \cdot (\mathbf{V}u - D\nabla u) = f(x,t), & x \in \Omega,\ t \in (0,T] \\ \text{Appropriate boundary conditions} \\ u(x,0) = u_0(x) \end{cases} \tag{2.1}$$

where $\Omega = [a, b]$ is an interval with boundary $\Gamma := \partial\Omega$, $u(x,t)$ is the unknown function, $\mathbf{V}(x,t)$ is a velocity field, $D(x,t)$ is a diffusion coefficient, and $f(x,t)$ is a source/sink term.

Let Γ^I, Γ^O, and Γ^N be the inflow, outflow, and noflow boundaries identified by

$$\begin{aligned} \Gamma^I &:= \{x \mid x \in \Gamma, \mathbf{V}\cdot\mathbf{n} < 0\}, \\ \Gamma^O &:= \{x \mid x \in \Gamma, \mathbf{V}\cdot\mathbf{n} > 0\}, \\ \Gamma^N &:= \{x \mid x \in \Gamma, \mathbf{V}\cdot\mathbf{n} = 0\}, \end{aligned} \tag{2.2}$$

where $\mathbf{n}$ is the outward unit normal vector ($\mathbf{n} = 1$ or $\mathbf{n} = -1$ for one-dimensional space). The ELLAM framework can treat any boundary conditions [6, 16], but we restrict ourselves to the following boundary and initial conditions that are typical in applications:

$$\begin{aligned} u(x,t) &= g^O(x,t), && x \in \Gamma^O, && t \in [0,T], \\ (\mathbf{V}u - D\nabla u)(x,t)\cdot\mathbf{n} &= g^I(x,t), && x \in \Gamma^I, && t \in [0,T], \\ -D\nabla u(x,t)\cdot\mathbf{n} &= 0, && x \in \Gamma^N, && t \in [0,T], \\ u(x,0) &= u_0(x), && x \in \Omega. \end{aligned} \tag{2.3}$$

Let $0 = t_0 < t_1 < \cdots < t_{n-1} < t_n < \cdots < t_N = T$ be a partition of $[0,T]$ with $\Delta t_n := t_n - t_{n-1}$. We multiply Equation (2.1) by test functions $w(x,t)$ that vanish outside the space-time strip $\Omega \times (t_{n-1}, t_n]$ and are discontinuous in time at time t_{n-1}. Then, integration by parts leads us to the following weak form:

$$\begin{aligned} &\int_a^b u(x,t_n)w(x,t_n)\,dx + \int_{t_{n-1}}^{t_n}\int_a^b (D\nabla u)\cdot\nabla w\,dx\,dt \\ &\quad + \int_{t_{n-1}}^{t_n}\int_{\partial\Omega} (\mathbf{V}u - D\nabla u)\cdot\mathbf{n}w\,dS\,dt - \int_{t_{n-1}}^{t_n}\int_a^b u(w_t + \mathbf{V}\cdot\nabla w)\,dx\,dt \\ &= \int_a^b u(x,t_{n-1})w(x,t_{n-1}^+)\,dx + \int_{t_{n-1}}^{t_n}\int_a^b (fw)(x,t)\,dx\,dt, \end{aligned} \tag{2.4}$$

where dS is the differential element on $\partial\Omega$ and $w(x,t_{n-1}^+) := \lim_{t\to t_{n-1}^+} w(x,t)$ takes into account the fact that $w(x,t)$ are discontinuous in time at time t_{n-1}.

ELLAM takes advantage of the hyperbolic nature of convection-diffusion differential equations to require test functions to satisfy the adjoint equation

$$w_t + \mathbf{V}\cdot\nabla w = 0. \tag{2.5}$$

This cancels the last term on the left side of the weak form and implies that test functions are constants along characteristics defined by initial value problems to ordinary differential equations

$$\begin{cases} \dfrac{dy}{ds} = \mathbf{V}(y(s;x,t),s), \\ y(s;x,t)|_{s=t} = x. \end{cases} \tag{2.6}$$

For convenience, we denote $\Gamma_n^I := \Gamma^I \times [t_{n-1}, t_n]$, $\Gamma_n^O := \Gamma^O \times [t_{n-1}, t_n]$, and $\Gamma_n^N := \Gamma^N \times [t_{n-1}, t_n]$. For any $x \in \Omega$, if (x, t_n) backtracks along a characteristic to $(x^*, t^*) \in \Gamma_n^I$ or Ω at time t_{n-1}, we define $\Delta t^I(x,t_n) := t_n - t^*$ or $t_n - t_{n-1}$, respectively. Similarly, for any $(y,t) \in \Gamma_n^O$,

if it backtracks to $(y^*, t^*) \in \Gamma_n^I$ or Ω at time t_{n-1}, we define $\Delta t^O(y,t) := t - t^*$ or $t_n - t_{n-1}$, respectively.

By enforcing the backward Euler quadrature on Ω at time t_n and Γ_n^O, we obtain

$$\int_{t_{n-1}}^{t_n}\int_a^b f(x,t)w(x,t)\,dx\,dt = \int_a^b \Delta t^I(x,t_n) f(x,t_n)\, w(x,t_n)\,dx + \int_{\Gamma_n^O} \Delta t^O(y,t) f(y,t) w(y,t)\,(\mathbf{V}\cdot\mathbf{n})\,dS\,dt + E(f,w).$$

Similarly, the diffusion term can be evaluated as

$$\begin{aligned}&\int_{t_{n-1}}^{t_n}\int_a^b ((D\nabla u)\cdot\nabla w)(x,t)\,dx\,dt \\ &\quad = \int_a^b \Delta t^I(x,t_n)((D\nabla u)\cdot\nabla w)(x,t_n)\,dx \\ &\qquad + \int_{\Gamma_n^O} \Delta t^O(y,t)((D\nabla u)\cdot\nabla w)(y,t)\,(\mathbf{V}\cdot\mathbf{n})\,dS\,dt + E(D,u,w).\end{aligned}$$

Here $E(f,w)$ and $E(D,u,w)$ are truncation error terms.

The two formulas above rely on the backward Euler quadrature to approximate the corresponding integrals in weak form (2.4). It should be pointed out that higher order numerical quadratures have also been used to establish the ELLAM formulation [19].

Dropping the error terms in the source and diffusion terms and breaking up the boundary term, we obtain the following weak formulation: Find $u(x,t) \in H^1(\Omega \times (t_{n-1}, t_n])$ such that for any $w(x,t) \in H^1(\Omega \times (t_{n-1}, t_n])$ satisfying the adjoint equation (2.5), the following holds

$$\begin{aligned}&\int_a^b u(x,t_n)w(x,t_n)\,dx + \int_a^b \Delta t^I(x,t_n)(D\nabla u\cdot\nabla w)(x,t_n)\,dx \\ &\quad + \int_{\Gamma_n^O} \Delta t^O(y,t)(D\nabla u)\cdot\nabla w)(y,t)\,(\mathbf{V}\cdot\mathbf{n})\,dS\,dt \\ &\quad + \int_{\Gamma_n^O} (\mathbf{V}u - D\nabla u)\cdot\mathbf{n}\, w(y,t)\,dS\,dt + \int_{\Gamma_n^I} (\mathbf{V}u - D\nabla u)\cdot\mathbf{n}\, w(y,t)\,dS\,dt \\ &= \int_a^b u(x,t_{n-1})w(x,t_{n-1}^+)\,dx + \int_a^b \Delta t^I(x,t_n) f(x,t_n) w(x,t_n)\,dx \\ &\quad + \int_{\Gamma_n^O} \Delta t^O(y,t) f(y,t) w(y,t)\,(\mathbf{V}\cdot\mathbf{n})\,dS\,dt. \qquad (2.7)\end{aligned}$$

III. CHUI-QUAK SPLINE WAVELETS ON BOUNDED INTERVALS

During the late 1980s and early 1990s, a variety of wavelets with different properties were developed for applications of different types. Orthogonal wavelets usually do not have closed forms, and hence are difficult to be applied directly to boundary value problems or higher order differential equations. In this article, we shall use the semi-orthogonal spline wavelets constructed by Chui and Quak [11] to solve boundary value problems of convection-diffusion equations. For

TABLE I. Nodal values of linear Chui-Quak wavelets $\psi_{j,k}$.

Level-$(j+1)$ node	$2k-4$	$2k-3$	$2k-2$	$2k-1$	$2k$	$2k+1$	$2k+2$
Left ($k=1$), $\frac{1}{12}*$	N/A	N/A	12	−11	6	−1	0
Internal ($2 \le k \le 2^j-1$), $\frac{1}{12}*$	0	−1	6	−10	6	−1	0
Right ($k=2^j$), $\frac{1}{12}*$	0	−1	6	−11	12	N/A	N/A

semi-orthogonal wavelets, as will be seen later on, orthogonality is lost on the same scale, but still kept among different scales.

Let $j(\ge 1)$ be a positive integer and the unit interval $[0,1]$ be partitioned into 2^j dyadic cells. The dyadic nodes are $k/2^j, k = 0,1,\ldots,2^j$. For convenience, let us denote $Y_j = \{1,2,\ldots,2^j\}$ and $Z_j = \{0,1,2,\ldots,2^j\}$. Let V_j be the space of piecewise linear polynomials, i.e., linear splines over this dyadic partition. We define $\phi_{j,k}(x)$ as the linear nodal basis functions over this partition. For $k = 0$ or $k = 2^j$, we take only the half inside the unit interval $[0,1]$. It can be verified that [11]:

- $V_j = \text{span}\{\phi_{j,k}\}$;
- $V_j \subset V_{j+1}$, $\overline{\bigcup_{j\ge 1}^{\infty} V_j} = L^2(0,1)$.

Let W_{j+1} be the L^2-orthogonal complement of V_j in V_{j+1}, that is,

$$V_j \oplus W_{j+1} = V_{j+1}, \tag{3.1}$$

then $\dim W_{j+1} = 2^j$. In [11], a set of semi-orthogonal linear spline wavelets $\psi_{j,k}, k \in Y_j$ was constructed as a set of basis functions for W_j. Table I lists the nodal values of these linear Chui-Quak wavelets: left boundary, internal, and right boundary. Their graphs are shown in Fig. 1. Clearly, internal wavelet $\psi_{j,k}(x)$ is centered in the kth element of level j.

The two-scale equations for the internal scaling functions and wavelets are

$$\phi_{j,k} = \frac{1}{2}\phi_{j+1,2k-1} + \phi_{j+1,2k} + \frac{1}{2}\phi_{j+1,2k+1}, \tag{3.2}$$

$$\psi_{j,k} = -\frac{1}{12}\phi_{j+1,2k-3} + \frac{1}{2}\phi_{j+1,2k-2} - \frac{5}{6}\phi_{j+1,2k-1} + \frac{1}{2}\phi_{j+1,2k} - \frac{1}{12}\phi_{j+1,2k+1}. \tag{3.3}$$

Similar equations can be derived for the left and right boundary scaling functions and wavelets without any difficulty.

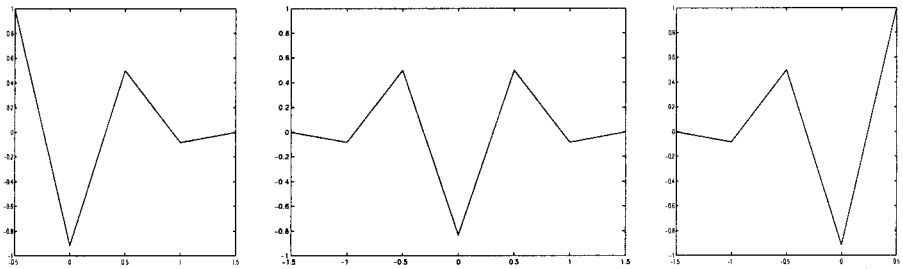

FIG. 1. Linear Chui-Quak wavelets.

The semi-orthogonality means

$$V_{j_1} \perp W_{j_2} \quad \text{if } j_1 \le j_2 \qquad \text{and} \qquad W_{j_1} \perp W_{j_2} \quad \text{if } j_1 \ne j_2,$$

that is,

$$(\phi_{j_1,k_1}, \psi_{j_2,k_2}) = 0 \quad \text{if } j_1 \le j_2 \qquad \text{and} \qquad (\psi_{j_1,k_1}, \psi_{j_2,k_2}) = 0 \quad \text{if } j_1 \ne j_2.$$

Furthermore, direct calculations give us

$$\left[(\phi_{j,k_1}, \phi_{j,k_2})_{k_1,k_2 \in Z_j}\right] = \frac{1}{2^j}\frac{1}{6}\begin{bmatrix} 2 & 1 & 0 & \cdots & 0 & 0 \\ 1 & 4 & 1 & \cdots & 0 & 0 \\ \cdots & \cdots & \cdots & \cdots & \cdots & \cdots \\ 0 & 0 & 0 & \cdots & 4 & 1 \\ 0 & 0 & 0 & \cdots & 1 & 2 \end{bmatrix} \tag{3.4}$$

and

$$\left[(\psi_{j,k_1}, \psi_{j,k_2})_{k_1,k_2 \in Y_j}\right] = \frac{1}{2^{j+1}}\frac{1}{108}\begin{bmatrix} 64 & 9 & -1 & 0 & 0 & \cdots & 0 & 0 & 0 & 0 & 0 \\ 9 & 54 & 10 & -1 & 0 & \cdots & 0 & 0 & 0 & 0 & 0 \\ -1 & 10 & 54 & 10 & -1 & \cdots & 0 & 0 & 0 & 0 & 0 \\ \cdots & \cdots & \cdots & \cdots & \cdots & \cdots & \cdots & \cdots & \cdots & \cdots & \cdots \\ 0 & 0 & 0 & 0 & 0 & \cdots & -1 & 10 & 54 & 10 & -1 \\ 0 & 0 & 0 & 0 & 0 & \cdots & 0 & -1 & 10 & 54 & 9 \\ 0 & 0 & 0 & 0 & 0 & \cdots & 0 & 0 & -1 & 9 & 64 \end{bmatrix}. \tag{3.5}$$

The Galerkin formulation for diffusion problems involves first-order derivatives of trial and test functions, so we also list the derivatives of these spline wavelets in Table II. The inner products of the derivatives of these splines can be computed directly, as well.

Applying (3.1) recursively, we obtain a multilevel subspace decomposition

$$V_{j_c} \oplus W_{j_c} \oplus \cdots \oplus W_{j_f-1} = V_{j_f}.$$

Hence, we have two bases for subspace V_{j_f}:

- The finest level scaling functions: $\phi_{j_f,k}, k \in Z_{j_f}$;
- The coarsest level scaling functions $\phi_{j_c,k}, k \in Z_{j_c}$, plus fine level wavelets $\psi_{j,k}$, $k \in Y_j$, $j_c \le j \le j_f - 1$.

Therefore, there are two equivalent representations for any function $f \in V_{j_f}$:

$$\sum_{k \in j_f} c_{j_f,k}\phi_{j_f,k} = \sum_{k \in Z_{j_c}} c_{j_c,k}\phi_{j_c,k} + \sum_{j=j_c}^{j_f-1}\sum_{k \in Y_j} d_{j,k}\psi_{j,k}. \tag{3.6}$$

TABLE II. Derivatives of linear Chui-Quak wavelets $\psi_{j,k}$.

Level-$(j+1)$ cell	$2k-3$	$2k-2$	$2k-1$	$2k$	$2k+1$	$2k+2$
Left ($k=1$), 2^j*	N/A	N/A	$-23/6$	17/6	$-7/6$	1/6
Internal ($2 \le k \le 2^j-1$), 2^j*	$-1/6$	7/6	$-16/6$	16/6	$-7/6$	1/6
Right ($k=2^j$), 2^j*	$-1/6$	7/6	$-17/6$	23/6	N/A	N/A

When we carry out approximations from subspace V_{j_f}, the first part on the right side of the above equivalence provides a basic approximation. Then, the wavelet coefficients in the second part brings in progressive improvements (or details). But wavelet coefficients are small in the smooth regions of the function being approximated, and hence can be suppressed to save computations. This is the wavelet compression discussed in [20].

The following features of these semi-orthogonal spline wavelets are attractive:

- The semi-orthogonality of scaling functions and wavelets allows us to conduct progressive approximations;
- The superpositions in (3.6) are easy to implement because all basis functions are piecewise linear polynomials;
- These splines have explicit expressions and, thus, allow us to handle Sobolev H^1-inner products and impose boundary conditions directly;
- As will be seen later, the coefficient matrix of the derived discrete system is symmetric and has a clear block structure.

To construct scaling functions and wavelets on a general interval $[a, b]$, we only need to perform a simple coordinate transform $x = (b-a)X+a$, $X \in [0, 1]$ and utilize the above standard scalings and wavelets on $[0, 1]$.

IV. A MULTILEVEL WAVELET SCHEME FOR CONVECTION-DIFFUSION PROBLEMS

Rather than covering the most general initial boundary value problems for convection-diffusion equations stated in Section II, we consider a convection-diffusion equation with the homogeneous Dirichlet boundary condition

$$\begin{cases} u_t + \nabla \cdot (Vu - D\nabla u) = f(x,t), & x \in \Omega,\ t \in (0,T], \\ u|_{\partial\Omega} = 0, \\ u(x,0) = u_0(x), \end{cases} \tag{4.1}$$

where $\Omega = [a, b]$ is a finite interval. Let j_c, j_f be the coarsest and finest spatial resolution levels and $S_{j_f}(\Omega)$ be the subspace generated by piecewise linear polynomials over the dyadic partition at level j_f on the interval $[a, b]$. We construct an adaptive multilevel scheme as follows.

Part 1: Initial Approximation

For any given initial data $u_0(x) \in L^2([a, b])$, we find an approximation from subspace S_{j_f}:

$$U_0(x) = \sum_{k \in Z_{j_f}} c^0_{j_f,k}\, \phi_{j_f,k}. \tag{4.2}$$

This could be the interpolation at those level-$(j + 1)$ dyadic nodes or the best L^2-approximation from S_{j_f}, for which we solve a tri-diagonal linear system. Then we apply (3.2) and (3.3) recursively to decompose the scaling coefficients at the finest level j_f into scaling coefficients at the coarsest level j_c and wavelet coefficients at the levels in between. A threshold ε is prescribed for wavelet compression. For hard-thresholding, wavelet coefficients just below the threshold are set to zero,

but those just above are kept intact. As pointed out in [21], hard-thresholding induces numerical instabilities and can be remedied by soft-thresholding described as below:

$$\overline{d^0_{j,k}} := \begin{cases} 0 & \text{if } |d^0_{j,k}| < \varepsilon, \\ 2(|d^0_{j,k}| - \varepsilon)\ \mathrm{sign}(d^0_{j,k}) & \text{if } \varepsilon \le |d^0_{j,k}| \le 2\varepsilon, \\ d^0_{j,k} & \text{if } |d^0_{j,k}| \ge 2\varepsilon. \end{cases} \tag{4.3}$$

We end up with

$$\overline{U_0}(x) = \sum_{k\in Z_{j_c}} c^0_{j_c,k}\phi_{j_c,k}(x) + \sum_{j=j_c}^{j_f-1}\sum_{k\in\overline{Y}^0_j} \overline{d^0_{j,k}}\psi_{j,k}(x), \tag{4.4}$$

where $\overline{Y}^0_j$ is the significant wavelet coefficient index set

$$\overline{Y}^0_j := \left\{k \in Y_j : |d^0_{j,k}| \ge \varepsilon\right\} \tag{4.5}$$

at time $t_0 = 0$ for the remaining wavelet coefficients after the compression.

Part 2: Prediction

In a multilevel approximation, scaling coefficients describe the basic shape of the solution, whereas wavelet coefficients describe the smoothness/roughness of the solution. The significant coefficient wavelet index sets $\overline{Y}^{n-1}_j (j = j_c, \ldots, j_f - 1, n = 1, 2, \ldots, N)$ reveal the rough regions of the solution $\overline{U_{n-1}}(x)$. Note that the convection has a finite propagation speed and the diffusion is relatively small, so we can utilize the information from characteristics to predict where the singularities (e.g., steep flow fronts) will be at time step t_n. In other words, we track $\overline{Y}^{n-1}_j$ forward along characteristics from time t_{n-1} to time t_n to obtain the predicted significant wavelet coefficient index sets $\widehat{Y}^n_j$.

Part 3: Solution

Once $\widehat{Y}^n_j$ are determined, we define an adaptive trial and test function subspace $\widehat{S_{j_f}(\Omega)} \subset S_{j_f}(\Omega)$ by

$$\widehat{S_{j_f}(\Omega)} := \mathrm{Span}\left\{\{\phi_{j_c,k}\}_{k\in Y_{j_c}}, \{\psi_{j,k}\}_{k\in\widehat{Y}^n_j, j_c\le j\le j_f-1}\right\}. \tag{4.6}$$

Then we seek $\hat{U}_n(x) \in \widehat{S_{j_f}(\Omega)}$ with

$$\hat{U}_n(x) = \sum_{k\in Z_{j_c}} c^n_{j_c,k}\phi_{j_c,k}(x) + \sum_{j=j_c}^{j_f-1}\sum_{k\in\widehat{Y}^n_j} d^n_{j,k}\psi_{j,k}(x) \tag{4.7}$$

such that for any $w(x, t_n) \in \widehat{S_{j_f}(\Omega)}$, the following holds:

$$\begin{aligned} &\int_a^b \hat{U}_n(x)w(x,t_n)\,dx + \int_a^b \Delta t_n D\nabla\hat{U}_n(x)\cdot\nabla w(x,t_n)\,dx \\ &\quad = \int_a^b \overline{U_{n-1}}(x)w(x,t^+_{n-1})\,dx + \int_a^b \Delta t_n f(x,t_n)w(x,t_n)\,dx. \end{aligned} \tag{4.8}$$

To solve the above system, we need to assemble the following two sparse matrices: the mass matrix

$$M := \begin{bmatrix} (\phi_{j_c,k_1}, \phi_{j_c,k_2}) & \mathbf{0} \\ \mathbf{0} & (\psi_{j,k_1}, \psi_{j,k_2}) \end{bmatrix},$$

and the stiffness matrix

$$S := \begin{bmatrix} (\phi'_{j_c,k_1}, \phi'_{j_c,k_2}) & (\psi'_{j,k_1}, \phi'_{j_c,k_2}) \\ (\phi'_{j_c,k_1}, \psi'_{j,k_2}) & (\psi'_{j_1,k_1}, \psi'_{j_2,k_2}) \end{bmatrix}.$$

Part 4: Compression and then Superposition

At each time step $t_n, n = 1, \ldots, N$, a compression on wavelet coefficients in

$$\hat{U}_n(x) = \sum_{k \in Z_{j_c}} c^n_{j_c,k} \phi_{j_c,k}(x) + \sum_{j=j_c}^{j_f-1} \sum_{k \in \widehat{Y}^n_j} d^n_{j,k} \psi_{j,k}(x) \tag{4.9}$$

can be performed, just like that in Part 1. The compressed solution $\overline{U_n}(x)$ is then defined by (or assembled)

$$\overline{U_n}(x) = \sum_{k \in Z_{j_c}} c^n_{j_c,k} \phi_{j_c,k}(x) + \sum_{j=j_c}^{j_f-1} \sum_{k \in \overline{Y}^n_j} \overline{d^n_{j,k}} \psi_{j,k}(x). \tag{4.10}$$

Two remarks follow.

- As seen above, many of the ingredients in this scheme are consistent with those of the explicit and unconditionally stable wavelet schemes developed in [4, 5] for convection-reaction equations, which are first-order hyperbolic equations. However, this article is targeted at convection-dominated diffusion problems. The scheme is no longer explicit due to the diffusion term. However, the linear system in (4.8) is well-conditioned, because the diffusion is small.
- The first part on the right side of (4.7) provides a basic approximation. The significant wavelet coefficients in the second part appear only near the moving fluid fronts, so the second part of the right side of (4.7) brings in progressive improvements to the approximation. This way, the scheme resolves the moving steep fronts present in the solution accurately, adaptively, and efficiently. Furthermore, the fact that the integral of a wavelet is zero implies the compression conserves the total mass.

V. IMPLEMENTATION STRATEGIES AND NUMERICAL EXPERIMENTS

Listed below are some strategies used in implementing the scheme.

1. For a time-dependent problem, the initial condition is supposed to be known to a certain resolution. This resolution can be taken as the finest resolution level j_f in our scheme. Interestingly, the point values of the initial condition u_0 over the corresponding dyadic partition are also the coefficients in (4.2) (as the best L^2-approximation from V_{j_f}),

when u_0 is linearly interpolated at these points. We can apply the fast wavelet decomposition algorithm based on (3.2) and (3.3) to obtain the scaling and wavelet coefficients at coarser levels. Then wavelet compression follows. This is similar to a common practice in the image processing community by taking pixel values as scaling coefficients at the finest level, because the integral of a scaling function on its support can be normalized to one.

2. Because all basis functions are piecewise linear polynomials, we only need to assemble their nonzero nodal values. The superposition in (4.10) is straightforward and fast, and we can easily reconstruct $\overline{U_{n-1}}$ to the finest resolution level j_f.
3. The first term on the right side of (4.8) can be rewritten as

$$\int_a^b \overline{U_{n-1}}(x^*) J(x^*, x) w(x, t_n)\, dx$$

with (x^*, t_{n-1}) as the back-tracking image of (x, t_n) and $J(x^*, x)$ as the Jacobian. Clearly $\overline{U_{n-1}}(x^*) J(x^*, x)$ reflects the convection, i.e., the mass flowing from point x^* at time t_{n-1} to point x at time t_n. This means the singularity of $\overline{U_{n-1}}$ is transported from time t_{n-1} to time t_n. Because $\overline{U_{n-1}}$ is already reconstructed to the finest resolution level, we can use the technique used in item (1) to get the scaling coefficients at the finest level. Then the fast wavelet algorithm again produces the inner products of $\overline{U_{n-1}} J$ with the scalings and wavelets specified in (4.6). This is easier and also more accurate than applying quadratures directly to evaluate those integrals.
4. Soft-thresholding instead of hard-thresholding is used for wavelet compression, to retain numerical stability.

In the multilevel wavelet scheme presented in section IV, if the threshold is set to zero, then the approximation will be equivalent to that of a single-level scheme at the finest level. Conversely, if the threshold is relatively large, then all wavelet coefficients will be suppressed and the scheme becomes a single-level scheme at the coarsest level. When only single-level scaling functions are used in the approximation, the approximation order will be 2, because the approximants are piecewise linear polynomials. So the actual approximation accuracy of the multilevel scheme with wavelet compression sits in between those of the single-level schemes with the coarsest and finest level. Clearly, it depends on the thresholding parameter. To better measure the approximation accuracy of the multilevel scheme, we look at the relationship between the error and the number of terms (scaling functions and wavelets) being actually used. Obviously, the number of terms depends on the thresholding parameter. This is the n-term approximation or nonlinear approximation discussed in [21]. In this section, we shall perform numerical experiments and interpret the numerical results from the viewpoint of n-term approximation.

We now consider Equation (4.1) with $V(x, t) = 1 + cx$ (with c being a small constant) and $0 < D \ll 1$. The initial condition is specified as a Gaussian hill

$$u_0(x) = \exp\left(-\frac{(x - x_c)^2}{2\sigma^2}\right),$$

where $0 < x_c < 1$ and $\sigma > 0$ are the center and standard deviation, respectively. The corresponding exact solution is given by

$$u(x, t) = \frac{\sqrt{2}\sigma}{\sqrt{2\sigma^2 + 4Dt}} \exp\left(-\frac{(x - V(x, t)t)^2}{2\sigma^2 + 4Dt}\right),$$

TABLE III. Numerical results for initial condition.

j_c	j_f	ε	Terms in U_0	$\|U_0 - u_0\|_\infty$	$\|U_0 - u_0\|_2$
5	6	0.0	65	1.0003E−2	2.4944E−3
5	7	0.0	129	2.5017E−3	6.1189E−4
5	8	0.0	257	5.9513E−4	1.4541E−4
5	9	0.0	513	1.1922E−4	2.9069E−5
5	9	0.1	33	3.8666E−2	5.1978E−3
5	9	0.01	39	1.0453E−2	1.8813E−3
5	9	0.001	64	1.1414E−3	2.7526E−4
5	9	0.00018	129	2.7257E−4	7.4092E−5

with $f(x,t)$ in Equation (4.1) being computed accordingly. In the numerical results reported below, we took $[a,b] = [0,1], T = 0.5, c = 0.01, D = 10^{-4}, x_c = 0.25, \sigma = 0.0447$, and $\Delta t = 0.1$. In the Tables III and IV, U_0 stands for the numerical solution at the initial time and U_T is the numerical solution at the final time T.

From Table III, we can observe the second-order convergence for the initial approximations. This is right, because the approximants are piecewise linear polynomials. Comparing the first two lines with the last two lines in Table III, we find that they use almost the same numbers of terms, but the results with nonlinear approximations are much better. The numerical results for the final solution with wavelet compression are listed in Table IV.

VI. CONCLUDING REMARKS

The wavelet scheme established in this article is also a finite element method. We have uniform (dyadic) partitions at different levels on the given interval. Each dyadic cell is a finite element, and the shape function is a linear polynomial. For finite element methods, the assembly is usually element oriented. But for wavelet methods, the superposition is usually node oriented.

In this article, we focus on Dirichlet boundary conditions for ease of presentation. But the method can be extended to other types of boundary conditions. For Neumann or Robin (total flux) boundary problems of second-order differential equations, first-order derivatives are involved in the boundary conditions. Since the derivatives of Chui-Quak linear spline wavelets are piecewise constants and all types of boundary conditions are already incorporated in the ELLAM formulation, we only need to modify those boundary integral terms in (2.7) for the wavelets touching the boundaries.

The extension of the multilevel scheme proposed in this article to multidimensional problems is basically technical. A direct approach is to construct tensor products of wavelets

TABLE IV. Numerical results with compression.

j_c	j_f	ε	Terms in U_0	$\|U_0 - u_0\|_\infty$	$\|U_0 - u_0\|_2$	Terms in U_T	$\|U_T - u_T\|_\infty$	$\|U_T - u_T\|_2$
5	9	1E−1	33	3.8666E−2	5.1978E−3	33	3.6084E−2	4.8587E−3
5	9	1E−2	39	1.0453E−2	1.8813E−3	37	2.2402E−2	3.5767E−3
5	9	1E−3	64	1.1414E−3	2.7526E−4	66	1.1012E−2	2.3003E−3
5	9	1.8E−4	129	2.7257E−4	7.4092E−5	126	1.0550E−2	2.2839E−3

and multiresolution analyses, if the domain is logically rectangular. For polygonal domains in the 2- or 3-dimensional spaces, we might apply the C^1-spline wavelets developed by S. T. Liu [22].

J. L. thanks Professors Charles Chui and Wenjie He for the inspiring discussions.

References

1. A. Barinka, T. Barsch, P. Charton, A. Cohen, S. Dahlke, W. Dahmen, and K. Urban, Adaptive wavelet schemes for elliptic problems—implementation and numerical experiments, SIAM J Sci Comput 23 (2001), 910–939.
2. Z. Chen, C. A. Micchelli, and Y. Xu, Discrete wavelet Petrov-Galerkin methods, Adv Comput Math 16 (2002), 1–28.
3. J. C. Goswami, A. K. Chan, and C. K. Chui, On solving first-kind integral equations using wavelets on a bounded interval, IEEE Trans, Antennas and Propagation 43 (1995), 614–622.
4. R. E. Ewing, J. Liu, and H. Wang, Adaptive biorthogonal spline schemes for advection-reaction equations, J Comput Phys 193 (2003), 21–39.
5. H. Wang and J. Liu, Development of CFL-Free, explicit schemes for multidimensional advection-reaction equations, SIAM J Sci Comput 23 (2001), 1418–1438.
6. M. A. Celia, T. F. Russell, I. Herrera, and R. E. Ewing, An Eulerian-Lagrangian localized adjoint method for the advection-diffusion equation, Adv Water Resour 13 (1990), 187–206.
7. I. Daubechies, Orthogonal bases of compactly supported wavelets, Comm Pure Appl Math 41 (1988), 909–996.
8. A. Cohen, I. Daubechies, and J.-C. Feauveau, Biorthogonal bases of compactly supported wavelets, Comm Pure Appl Math 45 (1992), 485–560.
9. D. Xiu and G. E. Karniadakis, A semi-Lagrangian high-order method for Navier-Stokes equations, J Comput Phys 172 (2001), 658–684.
10. W. Dahmen and C. A. Micchelli, Using the refinement equation for evaluating integrals of wavelets, SIAM J Numer Anal 30 (1993), 507–537.
11. C. K. Chui and E. Quak, Wavelets on a bounded interval, Numerical methods in approximation theory, Vol. 9, Internat Ser Numer Math 105, Birkhäuser, Basel, 1992, 53–75.
12. R. D. Nevels, J. C. Goswami, and H. Tehrani, Semi-orthogonal versus orthogonal wavelet basis sets for solving integral equations, IEEE Trans, Antennas Propagation 45 (1997), 1332–1339.
13. G. Nævdal, T. Mannseth, K. Brusdal, and J. E. Nordtvedt, Multiscale estimation with spline wavelets with application to two-phase porous-media flow, Inv Prob 16 (2000), 315–332.
14. D. Castano and A. Kunoth, Robust regression of scattered data with adaptive spline-wavelets, SFB 611 Preprint No.172, Universität Bonn, 2004.
15. K. Bittner and K. Urban, Adaptive wavelet methods using semiorthogonal spline wavelets: sparse evaluation of nonlinear functions, Preprint, University of Ulm, Germany, 2004.
16. H. Wang, H. K. Dahle, R. E. Ewing, M. S. Espedal, R. C. Sharpley, and S. Man, An ELLAM scheme for advection-diffusion equations in two dimensions, SIAM J Sci Comput 20 (1999), 2160–2194.
17. L. Wu and H. Wang, An Eulerian-Lagrangian single-node collocation method for transient advection-diffusion equations in multiple space dimensions, Numer Meth PDEs 20 (2004), 284–301.
18. T. F. Russell and M. A. Celia, An overview of research on Eulerian-Lagrangian localized adjoint methods (ELLAM), Adv Water Res 25 (2002), 1215–1231.

19. H. Wang, M. Al-Lawatia, and S. A. Telyakovskiy, Runge-Kutta characteristic methods for first-order linear hyperbolic equations, Numer Meth PDEs 13 (1997), 617–661.

20. R. A. DeVore, B. Jawerth, and V. Popov, Compression of wavelet decomposition, Am J Math 114 (1992), 737–785.

21. R. A. DeVore, Nonlinear approximation, Acta Numer 7 (1998), 51–150.

22. S. T. Liu, Quadratic stable wavelet bases on general meshes, Appl Comput Harmonic Anal, to appear.